Energy Flow in Thin Shell Implosions and Explosions

J. J. Ruby,[1,2] J. R. Rygg,[1,2,3] D. A. Chin,[1,2] J. A. Gaffney,[4] P. J. Adrian,[5] C. J. Forrest,[2] V. Yu. Glebov,[2] N. V. Kabadi,[5] P. M. Nilson,[2] Y. Ping,[4] C. Stoeckl,[2] and G. W. Collins[1,2,3]

[1]*Department of Physics and Astronomy, University of Rochester, Rochester, New York 14627, USA*
[2]*Laboratory for Laser Energetics, University of Rochester, Rochester, New York 14627, USA*
[3]*Department of Mechanical Engineering, University of Rochester, Rochester, New York 14627, USA*
[4]*Lawrence Livermore National Laboratory, Livermore, California 94550, USA*
[5]*Plasma Science and Fusion Center, Massachusetts Institute of Technology, Cambridge, Massachusetts 02139, USA*

(Received 26 August 2020; accepted 30 October 2020; published 18 November 2020)

Energy flow and balance in convergent systems beyond petapascal energy densities controls the fate of late-stage stars and the potential for controlling thermonuclear inertial fusion ignition. Time-resolved x-ray self-emission imaging combined with a Bayesian inference analysis is used to describe the energy flow and the potential information stored in the rebounding spherical shock at 0.22 PPa (2.2 Gbar or billions of atmospheres pressure). This analysis, together with a simple mechanical model, describes the trajectory of the shell and the time history of the pressure at the fuel-shell interface, ablation pressure, and energy partitioning including kinetic energy of the shell and internal energy of the fuel. The techniques used here provide a fully self-consistent uncertainty analysis of integrated implosion data, a thermodynamic-path independent measurement of pressure in the petapascal range, and can be used to deduce the energy flow in a wide variety of implosion systems to petapascal energy densities.

DOI: 10.1103/PhysRevLett.125.215001

Dynamic compression experiments [1–4] allow physics to be studied under conditions otherwise unobtainable on Earth, and in doing so, have pushed the boundaries of modern physics theory. Although these systems are described as high energy density (HED, also known as high pressure), the energy density (pressure) is exceedingly difficult to measure, limiting experimental measurement of pressure to particular thermodynamic pathways, such as the Hugoniot [1,2,5], that allow the pressure to be constrained by measurements of other quantities. In the most-extreme cases convergent geometries [5–7] are used to amplify the energy density that is achievable, creating the conditions necessary to fuse the nuclei hydrogen isotopes [7–10]. These conditions are comparable to the states predicted within the deep interior of main-sequence stars [11,12] and the envelope of compact objects such as white dwarfs [13], where physical theories have never been experimentally tested. Advanced analysis techniques [14–18] are necessary to quantify the pressure and energy evolution within these systems, whether it be for fundamental HED science [5,12,13] or to better understand the performance of inertially confined fusion (ICF) plasmas [7–10].

In this Letter, a new analysis methodology for implosion experiments is used to make a path independent measurement of pressure up to and beyond 2 Gbar with a full error analysis through Monte Carlo techniques, using decompression measurements of a laser-driven glass shell. A self-consistent mechanical model of the shell is combined with Bayesian inference techniques to infer the trajectory of the shell, the pressure profile at the fuel-shell interface, the ablation pressure, and the temporal history of the mechanical energies in the system. Such an *in situ* measurement of the energy evolution is used to quantitatively characterize the imploding system at gigabar pressures. This method can be applied to a variety of different implosion types to understand the assembled states of matter. The information gained from this single integrated measurement on an implosion experiment presents the first example of a self-consistent quantitative analysis of a convergent HED experiment at gigabar pressures with a robust uncertainty analysis.

The experiments were carried out at the University of Rochester's Laboratory for Laser Energetics [19]. A strong, spherically symmetric shock wave was launched into a 3-μm-thick SiO_2 shell of 879 μm outer diameter, a so-called "direct-drive exploding-pusher" target [20], filled with nearly 20 atm of deuterium gas (D_2). A schematic of the experiment is shown in Fig. 1(a). The shock [gold dashed in Fig. 1(a)] was launched by using approximately 14 kJ of ultraviolet laser light from the 60-beam OMEGA laser with a 600-ps super-Gaussian temporal profile shown in Fig. 1(b). The beams used SG5 distributed phase plates providing, a super-Gaussian spot with a diameter of around 720 μm [21].

The absorbed laser light ablates the surface of the shell and drives a shock wave into the target [20]. This shock wave transits through the shell, imparting momentum radially inward. The shock, after breaking out and into

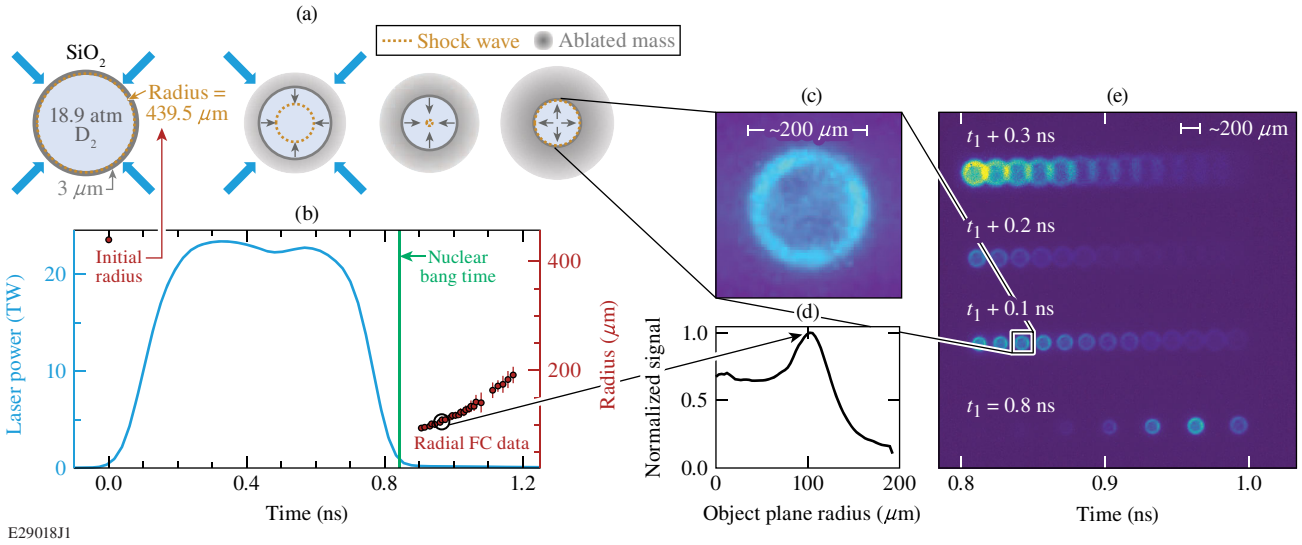

FIG. 1. (a) Schematic of the experimental setup, showing a 3-μm SiO_2 shell filled with 18.9 atm of D_2 gas. Symmetric laser illumination drives a shock wave (dashed gold curve) through the shell into the gas and the shell continues to converge. The shock wave reaches the center of the target and then returns moving outward and eventually interacts with the shell a second time. (b) The time history of the laser drive and measurements along with the time that the shock reaches the center of the target given by the nuclear bang time (vertical green line), a measurement of thermonuclear fusion products due to the extreme temperatures and densities created by the converging shock wave. When the rebounding shock wave interacts with the shell, the conditions generate the x rays (e) measured in the roughly 30-ps snapshots. (d) The peak of the radially averaged lineouts corresponds to the ring of emission in the (c) individual snapshot and the red data points shown in (b).

the deuterium gas, converges to the center of the target, producing a steep increase in pressure, temperature, and density. The shock then moves outward, decaying, and eventually colliding with the converging shell. Once the expanding shock hits the imploding shell, the shell reverses direction and begins to move outward. The SiO_2 shell's temperature becomes sufficiently high to ionize and produce significant bremsstrahlung emission. This emission is measured using a 46-pinhole array attached to a time-gated Sydor x-ray framing camera [22], providing a 2D projection of the emitting shell with multiple temporal snapshots.

The framing-camera measurements were taken with an array of 10-μm pinholes at a magnification of 6. The images from the pinholes are projected onto the voltage gated x-ray detector and swept in time, giving snapshots of the x-ray emission over approximately a 30-ps temporal integration as determined from the voltage sweep, shown in Fig. 1(e). The emission is localized in space and radially symmetric indicating that a well-defined shell of mass is present.

The center of each image is located, and the peak of the radially averaged lineout is taken as the position of the shell. An example frame and lineout are shown in Figs. 1(c) and 1(d), respectively. The time corresponding to this position is calculated and the trajectory determined, as shown in Fig. 2(b) in red points alongside the temporal profile of the laser pulse (blue curve) and the time of peak neutron emission (vertical green line) which corresponds to roughly when the shock is at the center of the target.

The "thin shell" model [23] used to describe the system treats the shell mass as localized in space and considers the pressure pushing the shell inward (P_{abl}), to smaller radii, by mass ablation and the pressure pushing the shell outward

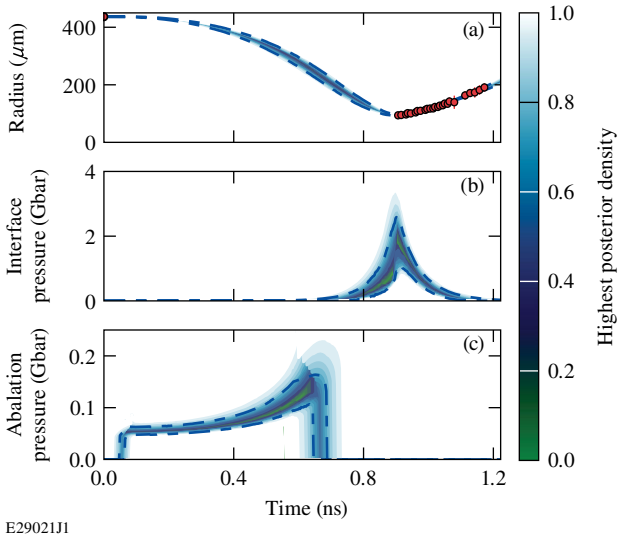

FIG. 2. The inferred (a) shell trajectory, (b) pressure at fuel shell interface, and (c) ablation pressure resulting from Bayesian parameter estimation based on the experimentally measured data. Color bar shows highest posterior density intervals for each quantity with the 68.3% credible interval given by the dashed line in each.

(P_{fuel}), to larger radii, due to the internal energy of the compressed fuel. The balance of these pressures is used to calculate the force on the shell, and therefore the acceleration through Newton's second law. The trajectory of the shell is found by integrating the second-order ordinary differential equation,

$$\frac{d^2R}{dt^2} = \frac{4\pi R^2(P_{\text{fuel}} - P_{\text{abl}})}{M_{\text{shell}}}, \tag{1}$$

where R is the radial location of the shell and the acceleration of the shell is given by the net pressure times the area of the shell divided by the mass of the shell (M_{shell}). The temporal mass profile is based on a constant ablation rate and, in conjunction with an exhaust velocity, this sets the inward pressure felt by the shell due to the rocket effect of mass ablation. The outward pressure felt by the shell is modeled by exponential growth and decay before and after the rebounding shock reaches the shell, respectively.

This model [24] is derived from similar models evoked to interpret x-ray-driven implosion experiments [8,9] with a few modifications that are specific to exploding pushers. These targets have low shell mass and the energy transport into the fuel is dominated by shock heating, rather than compressive heating. The small remaining mass of the shell is why the rebounding shock is able to change the direction of the shell in the experiment. This system is able to reach similar pressures as more compressive experiments but does so with low convergence.

The model, as part of a Bayesian inference framework, is used to deduce interesting physical quantities from the integrated measurements. This process was verified [24] using synthetic data generated from the 1D hydrodynamics code LILAC [25]. The Bayesian inference process constrains the self-consistent model, with a physically meaningful parametrization, using as much available information from the experiment as possible such as initial target conditions, physical conservation laws, and measurements. The model is efficient enough to be inverted using a sequential Monte Carlo [26] sampling of the likelihood surface, implemented using PYMC3 [27], and the full posterior distributions of the parameters are found. These distributions are then used to construct the experimentally informed distributions for the physical conditions present in the system shown in Figs. 2 and 3.

The experimentally inferred shell trajectory and temporal pressure profile at the fuel-shell interface and ablation front, Figs. 2(a)–2(c), are a direct result of the model inference. The trajectory [Fig. 2(a)] and ablation pressure [Fig. 2(c)] are both tightly constrained, at the 5% and 10% levels, respectively. Pressure is a key quantity that characterizes a HED system (as it is the measure of energy density), and specifically the ablation pressure is a measure of how efficiently laser energy couples into the converging shell. Ablation pressure is usually either measured in planar geometry [28] or inferred from hydrodynamics codes in spherical geometry [29], in both cases the utility for testing the coupling models for implosions is limited. These particular measurements are but one example of the utility provided by the richness and complexity of the results derived from this analysis method.

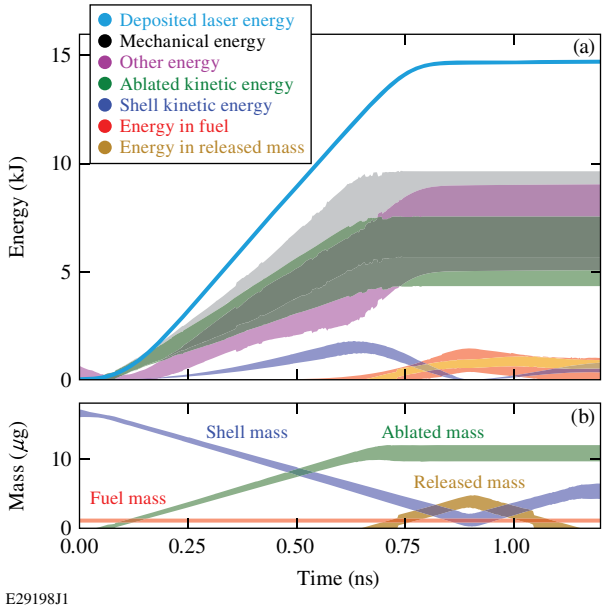

FIG. 3. (a) 68.3% credible intervals for the different energy components within the model. The energy components include shell kinetic energy (dark blue shading), total fuel energy (red shading), shell kinetic energy that does not to work on the fuel (gold shading), and ablated kinetic energy (green shading). Also shown is the total mechanical energy in the model (gray shading), the laser energy deposited (light blue shading), and the difference (magenta shading) being a measure of nonmechanical energy in the system including internal energy of the corona and shell, radiation losses, and uncoupled laser energy. The mechanical energy of the system accounts for approximately half of the total incident laser energy, but of that only about 10% contributes to doing work on the fuel. (b) Mass credible intervals from the model including the shell mass (dark blue shading), ablated mass (green shading), the released mass (gold shading), and the fuel mass (red shading) as a function of time.

The pressure profile in Fig. 2(b) shows a peak pressure of $2.2 \pm 0.7/1.0$ Gbar corresponding to the outgoing shock wave hitting the shell. The pressures measured here exceeds the energy density defined by binding energy of core electrons and the volume of their orbitals (≈500 Mbar for Si), meaning if there are still bound electrons (very likely prior to the return shock hitting the shell), their orbitals will be highly perturbed by neighboring atoms leading to complex collective behavior [30]. Beyond the direct pressure effects that may occur, measuring the pressure profile at the fuel shell interface, and specifically the pressure when the shock reaches the interface, is interesting for two reasons: (1) The direct measurement of pressure is one of the most challenging aspects

of making an absolute equation-of-state measurement, especially at gigabar conditions, and (2) in traditional (compressive) ICF implosions, the fuel is generally regarded as isobaric, so a measurement of the pressure at the fuel-shell interface gives the pressure of the entire fuel.

In addition to the pressure profiles, the use of a self-consistent mechanical model for the shell gives insight into how energy is partitioned throughout the experiment. The kinetic energy of the imploding shell follows from the velocity of the shell [calculated when solving Eq. (1)] and the mass of the shell, $E_{\mathrm{kin}} = 0.5Mv^2$, and the work done on the fuel by the shell follows from the trajectory of the shell and the pressure profile at the interface. The work dW at a given time is equal to the change in volume dV of the fuel (given by the position of the shell) multiplied by the pressure P at the boundary,

$$dW = PdV, \tag{2}$$

the total work done on the fuel and, assuming adiabatic compression, the total energy of the fuel, follows from integrating the work. There are additional forms of mechanical energy modeled and there are additional forms of energy not accounted for by the model, all of which are presented in Fig. 3(a). The solid blue line is the laser energy as a function of time, from integrating the measured on-shot power. The shaded regions represent the highest posterior density intervals with 68.3% of the probability for each of the energy components. Components constrained in the model include the shell kinetic energy (dark blue shading), the energy in the fuel (red shading), the kinetic energy of the ablated mass (green), and the kinetic energy of the shell which does not do work on the fuel due to material release (gold shading). The sum of these components (gray shading) represents the total mechanical energy in the system. The remaining difference between the mechanical energy and the total laser energy (magenta shading) represents all of the different energy sinks that are not captured in the model. These components include internal energy of the corona and shell, radiation losses, and uncoupled laser energy.

The mechanical energy of the system plateaus prior to the laser energy, showing the time when the shell decouples from the ablation surface. At this point, additional laser energy does not increase the kinetic energy of the shell and does not contribute to adding energy to the fuel. This point coincides with the peak of the kinetic energy of the shell, which is an important metric for the performance of ICF implosions, although it is rarely directly measured [9,31]. Additional laser energy deposited after this point likely stays in the already ablated mass in the form of thermal energy. Although about half of the incident laser energy goes into mechanical energy of the system, only about 10% of this energy ends up in the fuel. All of the shell mass does not contribute to doing work on fuel [32], demonstrated in Fig. 3(b) where the different mass components are shown as a function of time.

The mass that does work on the fuel is the shell mass, about 60% of which is ablated by the time the laser turns off, after which the mass from the shell begins to release. This released mass also does not do work on the fuel. Ultimately the shell changes direction when the pressure from the fuel is sufficiently high, at which point released mass is recaptured as the shell moves out.

Previous measurements of mechanical energy and mass remaining in implosion experiments rely on backlit radiography techniques [31,33], which are perturbative to the system and require the removal of drive beams reducing symmetry. They also often make use of hydrodynamics codes to infer system quantities making uncertainty analysis challenging [9,14,15,17]. The method developed here provides the peak kinetic energy of the shell, the complete time history of the kinetic energy of the shell, and the work done on the fuel in a nonperturbative, *in situ* measurement. The analysis technique provides a method for gaining quantitative insight from integrated HED measurements that was previously not possible.

To provide perspective, Fig. 4 shows a temperature-density diagram and a series of isobars (curves of constant pressure) corresponding to other relevant HED regimes such as 1 Mbar, the top pressure achieved in static compression experiments (with some exceptions) [34], 50 Mbar, the top pressures measured in planar dynamic experiments [35], 2.2 Gbar, the highest pressure measured in this experiment, and 300 Gbar, the pressure predicted to be in the core of the sun [11] and the highest predicted

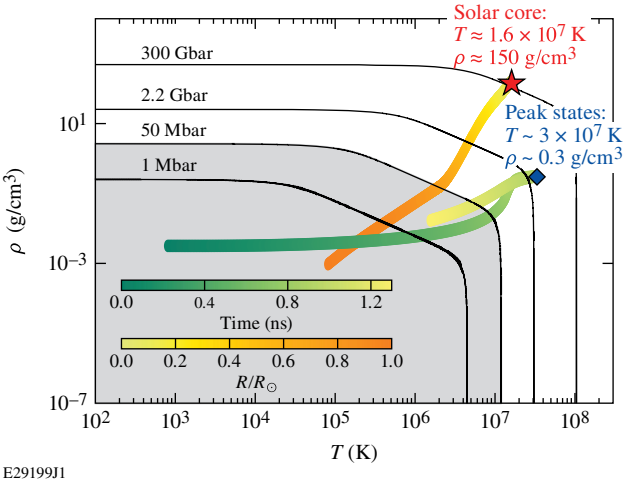

FIG. 4. A temperature-density diagram showing four isobars (black curves), predicted states found in the solar interior as a function of solar radius (orange color scale) and the states found in the fuel during the experiment presented here assuming an ideal equation of state. The gray shaded region is where most HED experimental measurements are historically made, generally below 50 Mbar.

pressures in HED experiments [8,9]. The orange-yellow color map shows the modeled temperature and density states as functions of radius within the solar interior [11]. The green-yellow color map shows the temperature and density states of the fuel in this experiment as functions of time derived from assuming a fully ionized ideal equation of state and conservation of mass using the trajectory of shell to determine fuel volume and the pressure at the interface, treating the fuel as isobaric, a reasonable approximation (due to the high temperatures, $> 10^6$ K, leading to high sound speeds) despite the spatial gradients likely within the temperature and density. This provides a useful illustration of the average temperature and density states within the fuel given the measured energy deposited within the fuel. Generally, as seen here, convergent HED systems reach pressures relevant to solar interiors but through higher temperatures and lower densities, although experimental designs can be tuned to achieve densities more relevant to stellar interiors.

In summary, the interaction of a laser-driven glass shell with a gigabar rebounding shock wave was studied using Bayesian inference and *in situ* x-ray self-emission imaging. The peak pressure achieved by the shock wave was $2.2 \pm 0.7/1.0$ Gbar, higher than any previous mechanical measurement of a shock wave strength. The measurement of ablation pressure and shell trajectory can both be used to test key physics used in implosion modeling and the full temporal history of the kinetic energy of the shell provides insight into both the efficiency of laser conversion into mechanical energy and ultimately into the work done on the fuel. The implications of these measurements are far reaching: the possibility of absolute equation-of-state measurements using a mechanical measurement of pressure [5], diagnosing the conditions within implosions for studies of atomic spectroscopy [36], fundamental nuclear science under extreme thermodynamic conditions [12], and more robust methods for quantifying the performance of ICF implosions [9,14,15,17]. The numerous results presented here demonstrate the richness of information that is available from Bayesian inference of integrated data from convergent HED experiments.

This material is based upon work supported by the Department of Energy National Nuclear Security Administration under Award No. DE-NA0003856, the U.S. Department of Energy, Office of Science, Fusion Energy Sciences under Award No. DE-SC0019269, the University of Rochester, and the New York State Energy Research and Development Authority. Y. P. acknowledges support from DOE OFES early career program and LLNL LDRD program. D. A. C. and P. J. A. acknowledge DOE NNSA SSGF support, which is provided under Cooperative Agreement No. DE-NA0003960. This Letter was prepared as an account of work sponsored by an agency of the U.S. Government. Neither the U.S. Government nor any agency thereof, nor any of their employees, makes any warranty, express or implied, or assumes any legal liability or responsibility for the accuracy, completeness, or usefulness of any information herein. The views and opinions of authors expressed herein do not necessarily state or reflect those of the U.S. Government or any agency thereof. Prepared by LLNL under Contract No. DE-AC52-07NA27344. This document was prepared as an account of work sponsored by an agency of the U.S. government. Neither the U.S. government nor Lawrence Livermore National Security, LLC, nor any of their employees makes any warranty, expressed or implied, or assumes any legal liability or responsibility for the accuracy, completeness, or usefulness of any information herein. The views and opinions of authors expressed herein do not necessarily state or reflect those of the U.S. government or Lawrence Livermore National Security, LLC, and shall not be used for advertising or product endorsement purposes.

[1] G. Collins, L. DaSilva, P. Celliers, D. Gold, M. E. Foord, R. Wallace, A. Ng, S. Weber, K. Budil, and R. Cauble, Science **281**, 1178 (1998).

[2] L. B. Da Silva, P. Celliers, G. W. Collins, K. S. Budil, N. C. Holmes, T. W. Barbee, Jr., B. A. Hammel, J. D. Kilkenny, R. J. Wallace, M. Ross *et al.*, Phys. Rev. Lett. **78**, 483 (1997).

[3] D. N. Polsin, D. E. Fratanduono, J. R. Rygg, A. Lazicki, R. F. Smith, J. H. Eggert, M. C. Gregor, B. H. Henderson, J. A. Delettrez, R. G. Kraus *et al.*, Phys. Rev. Lett. **119**, 175702 (2017).

[4] M. Millot, N. Dubrovinskaia, A. Cernok, S. Blaha, L. Bubrovinky, D. Braun, P. Celliers, G. Collins, J. Eggert, and R. Jeanloz, Science **347**, 418 (2015).

[5] T. Döppner, D. C. Swift, A. L. Kritcher, B. Bachmann, G. W. Collins, D. A. Chapman, J. Hawreliak, D. Kraus, J. Nilsen, S. Rothman *et al.*, Phys. Rev. Lett. **121**, 025001 (2018).

[6] S. Atzeni and J. M. ter vehn, *The Physics of Inertial Fusion Beam Plasma Interaction, Hydrodynamics, Hot Dense Matter*, 1st ed. (Oxford University Press, Oxford, 2004).

[7] M. R. Gomez, S. A. Slutz, A. B. Sefkow, D. B. Sinars, K. D. Hahn, S. B. Hansen, E. C. Harding, P. F. Knapp, P. F. Schmit, C. A. Jennings *et al.*, Phys. Rev. Lett. **113**, 155003 (2014).

[8] O. Hurricane, D. Callahan, D. Casey, P. Celliers, C. Cerjan, E. Dewald, T. R. Dittrich, T. Doppner, D. E. Hinkel, L. Berzak-Hopkins *et al.*, Nature (London) **506**, 343 (2014).

[9] S. LePape, L. Berzak-Hopkins, L. Divol, A. Pak, E. Dewald, S. Bhandarkar, L. Bennedetti, T. Bunn, J. Biener, J. Crippen *et al.*, Phys. Rev. Lett. **120**, 245003 (2018).

[10] V. Gopalaswamy, R. Betti, J. P. Knauer, N. Luciani, D. Patel, K. Woo, A. Bose, I. Igumenshchev, E. Campbell, K. Anderson *et al.*, Nature (London) **565**, 581 (2019).

[11] J. N. Bahcall, A. M. Serenelli, and S. Basu, Astrophys. J. **621**, L85 (2005).

[12] D. T. Casey, D. B. Sayre, C. R. Brune, V. A. Smalyuk, C. R. Weber, R. E. Tipton, J. E. Pino, G. Grim, B. A. Remington, D. Dearborn *et al.*, Nat. Phys. **13**, 1227 (2017).
[13] A. L. Kritcher, D. C. Swift, T. Dppner, B. Bachmann, L. X. Benedict, G. W. Collins, J. L. DuBois, F. Elsner, G. Fontaine, J. A. Gaffney *et al.*, Nature (London) **584**, 51 (2020).
[14] C. Cerjan, P. Springer, and S. Sepke, Phys. Plasmas **20**, 056319 (2013).
[15] J. Gaffney, D. Clark, V. Sonnad, and S. Libby, Nucl. Fusion **53**, 073032 (2013).
[16] P. Bremer, D. Malijovec, A. Saha, B. Wang, J. Gaffney, B. Spears, and V. Pascucci, Comput. Visual. Sci. **17**, 1 (2015).
[17] J. Gaffney, S. Brandon, K. Humbird, M. Kruse, R. Nora, J. Peterson, and B. Spears, Phys. Plasmas **26**, 082704 (2019).
[18] M. F. Kasim, T. P. Galligan, J. Topp-Mugglestone, G. Gregori, and S. M. Vinko, Phys. Plasmas **26**, 112706 (2019).
[19] T. Boehly, D. Brown, R. Craxton, R. Keck, J. Knauer, J. Kelly, T. Kessler, S. Kumpan, S. Loucks, S. Letzring *et al.*, Opt. Commun. **133**, 495 (1997).
[20] B. Ahlborn, M. H. Key, and A. R. Bell, Phys. Fluids **25**, 541 (1982).
[21] T. Kessler, Y. Lin, J. Armstrong, and B. Velazquez, Proc. SPIE Int. Soc. Opt. Eng. **1870**, 95 (1993).
[22] J. Kilkenny, Laser Part. Beams **9**, 49 (1991).
[23] M. M. Basko and J. Meyer-ter-Vehn, Phys. Rev. Lett. **88**, 244502 (2002).
[24] J. J. Ruby *et al.*, companion paper, Phys. Rev. E **102**, 053210 (2020).
[25] J. Delettrez, R. Epstein, M. C. Richardson, P. A. Jaanimagi, and B. L. Henke, Phys. Rev. A **36**, 3926 (1987).
[26] A. Doucet, N. de Freitas, and N. Gordon, *Sequential Monte Carlo Methods in Practice*, 1st ed. (Springger Science+Business Media, New York, 2001).
[27] J. Salvatier, T. V. Wiecki, and C. Fonnesbeck, Peer J. Comput. Sci. **2**, e55 (2016).
[28] D. E. Fratanduono, T. R. Boehley, P. M. Celliers, M. A. Barrios, J. H. Eggert, R. F. Smith, D. G. Hicks, G. W. Collins, and D. D. Meyerhofer, J. Appl. Phys. **110**, 073110 (2011).
[29] R. Nora, W. Theobald, R. Betti, F. J. Marshall, D. T. Michel, W. Seka, B. Yaakobi, M. Lafon, C. Stoeckl, J. Delettrez *et al.*, Phys. Rev. Lett. **114**, 045001 (2015).
[30] S. X. Hu, Phys. Rev. Lett. **119**, 065001 (2017).
[31] D. Hicks, B. Spears, D. Braun, R. Olson, C. Sorce, P. Celliers, G. Collins, and O. Landen1, Phys. Plasmas **17**, 102703 (2010).
[32] V. N. Goncharov, T. C. Sangster, R. Betti, T. R. Boehly, M. J. Bonino, T. J. B. Collins, R. S. Craxton, J. A. Delettrez, D. H. Edgell, R. Epstein *et al.*, Phys. Plasmas **21**, 056315 (2014).
[33] J. R. Rygg, O. S. Jones, J. E. Field, M. A. Barrios, L. R. Benedetti, G. W. Collins, D. C. Eder, M. J. Edwards, J. L. Kline, J. J. Kroll *et al.*, Phys. Rev. Lett. **112**, 195001 (2014).
[34] Z. Jenei, E. O'Bannon, S. Weir, H. Cynn, M. Lipp, and W. Evans, Nat. Commun. **9**, 3563 (2018).
[35] M. C. Marshall, A. E. Lazicki, D. Erskine, R. A. London, D. E. Fratanduono, P. M. Celliers, J. H. Eggert, F. Coppari, D. C. Swift, P. A. Sterne *et al.*, Phys. Rev. B **99**, 174101 (2019).
[36] J. E. Bailey, T. Nagayama, G. P. Loisel, G. A. Rochau, C. Blancard, J. Colgan, P. Cosse, G. Faussurier, C. J. Fontes, F. Gilleron *et al.*, Nature (London) **517**, 56 (2015).